NANO LETTERS

Letter

pubs.acs.org/NanoLett

Reduced Graphene Oxide Films with Ultrahigh Conductivity as Li-Ion Battery Current Collectors

Yanan Chen,[†] Kun Fu,[†] Shuze Zhu,[‡] Wei Luo,[†] Yanbin Wang,[†] Yiju Li,[†] Emily Hitz,[†] Yonggang Yao,[†] Jiaqi Dai,[†] Jiayu Wan,[†] Valencia A. Danner,[†] Teng Li,[‡] and Liangbing Hu*[,†]

[†]Department of Materials Science and Engineering and [‡]Department of Mechanical Engineering, University of Maryland, College Park, Maryland 20742, United States

Supporting Information

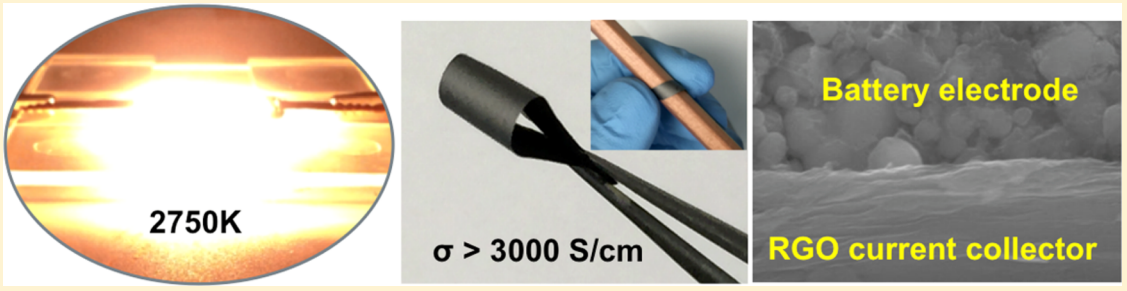

ABSTRACT: Solution processed, highly conductive films are extremely attractive for a range of electronic devices, especially for printed macroelectronics. For example, replacing heavy, metal-based current collectors with thin, light, flexible, and highly conductive films will further improve the energy density of such devices. Films with two-dimensional building blocks, such as graphene or reduced graphene oxide (RGO) nanosheets, are particularly promising due to their low percolation threshold with a high aspect ratio, excellent flexibility, and low cost. However, the electrical conductivity of these films is low, typically less than 1000 S/cm. In this work, we for the first time report a RGO film with an electrical conductivity of up to 3112 S/cm. We achieve high conductivity in RGO films through an electrical current-induced annealing process at high temperature of up to 2750 K in less than 1 min of anneal time. We studied in detail the unique Joule heating process at ultrahigh temperature. Through a combination of experimental and computational studies, we investigated the fundamental mechanism behind the formation of a highly conductive three-dimensional structure composed of well-connected RGO layers. The highly conductive RGO film with high direct current conductivity, low thickness (~4 μm) and low sheet resistance (0.8 Ω/sq.) was used as a lightweight current collector in Li-ion batteries.

KEYWORDS: *High conductivity, high-temperature reduction, reduced graphene oxide, current collector, lightweight, Li-ion batteries*

The need for lightweight, highly conductive films is ubiquitous in electronics and energy devices. For example, the current collectors used in Li ion batteries, made of copper (Cu) foil at the anode and of aluminum (Al) foil at the cathode, account for 15~50% of the total weight of the device.[1] In aqueous batteries (e.g., NiMH), current collectors account for ~6% of the weight and ~13% of the cost, yet they play a critical role in the electrochemical (EC) performance, particularly the EC stability of the battery and the interface stability of the electrodes. Current collectors used today in aqueous batteries (stainless steel (SS), titanium (Ti), nickel (Ni) foam, Ni-coated SS, and carbon cloth) are heavy, expensive, bulky, and prone to corrosion after prolonged use.[2,3] Competing technologies for battery current collectors have been developed, including carbon nanotube films, graphene films, graphene-coated metals, and flexible graphite foils.[4−9] However, efforts using these forms of nanocarbon have had limited success, especially in terms of conductivity and cost, and do not meet the requirement for practical batteries. Highly conductive carbon nanotube films have been reported for different applications from transparent electrodes to battery current collectors[10−13] but the application of low-cost carbon nanotubes to batteries remains to be explored. Two-dimensional graphene also shows promise as a low-cost alternative due to the abundance of its raw material, graphite. Freestanding films and composites with exfoliated graphene have been widely reported but the dc conductivity is usually limited to 100 S/cm due to the sheet−sheet junction resistance and small sheet sizes (usually around one micrometer).[14]

Reduced graphene oxide (RGO) nanosheets are extremely attractive due to their large lateral size (up to a few hundred micrometers) after processing, which results in a much lower percolation threshold and fewer junctions in a continuous film, giving rise to high electrical conductivity.[15,16] Various conductive nanostructures based on RGO have been reported

Received: February 20, 2016
Revised: April 22, 2016
Published: May 5, 2016

DOI: 10.1021/acs.nanolett.6b00743
Nano Lett. 2016, 16, 3616−3623

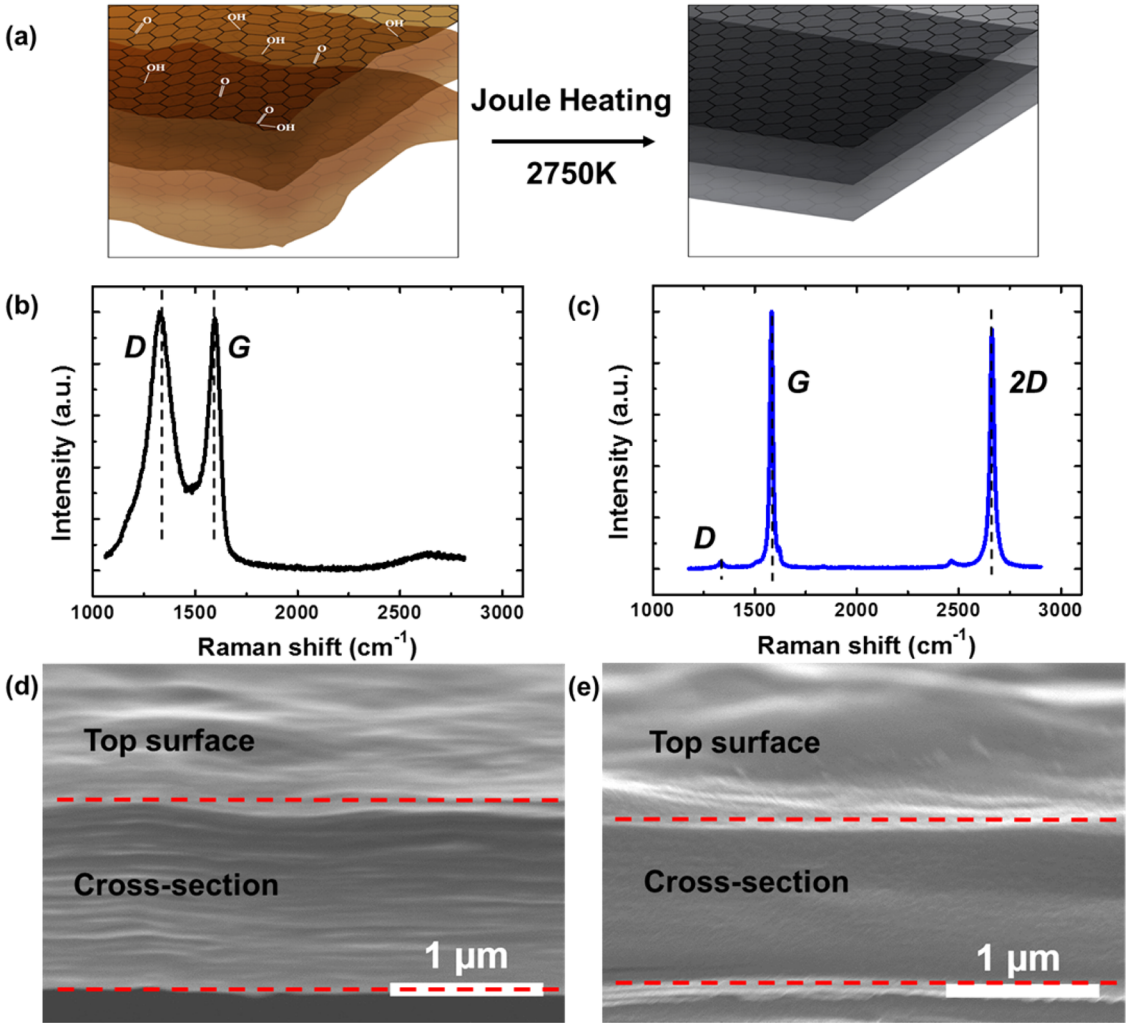

Figure 1. (a) Joule heating at 2750 K for 1 min in vacuum can effectively reduce the RGO, leading to a record-high dc conductivity. (b,c) Raman spectrum comparison of a RGO film annealed in a furnace at 773 K and the same film after the 2750 K annealing for 1 min, respectively. The low D/G ratio and the high 2D peak indicate highly crystalline RGO nanosheets after the process. (d,e) Cross-section SEM images of the RGO film before and after the Joule heating. The Joule heating effectively densifies the RGO films, which significantly increases the coupling in charge transport.

in the past ten years.[17−20] Achieving high-purity, close to pristine graphene through the reduction of graphene oxide (GO) is a major challenge, as the defects and functional groups in partially reduced RGO will largely impede carrier transport. Various reduction methods have been reported, including thermal reduction, chemical reduction and photochemical reduction.[21−27] Effective reduction can dramatically improve the electrical conductivity in RGO nanostructures. However, the highest dc conductivity reported in RGO nanostructure is typically less than 1000 S/cm. The low conductivity of the RGO films prohibits their use as current collectors in Li-ion batteries.

Joule heating is a straightforward method to process and modify carbon nanomaterials, and in particular has been widely explored in carbon nanotubes.[28,29] Selectively burning metallic carbon nanotubes in a carbon nanotube network can effectively increase the on/off current ratio of network-based transistors.[30−32] In this study, we applied Joule heating to effectively reduce GO at an ultrahigh temperature (~2750 K) in a short time (1 min), which led to a record high dc conductivity of 3112 S/cm. The high dc conductivity is related to the highly crystalline graphene structure formed by the high temperature annealing. The electrical current-induced high temperature can facilitate the thermal reduction of graphene oxides. Different from traditional thermal treatment in a furnace, Joule heating can generate ultrahigh temperature at junction points where the higher electrical resistance is located. The self-healing thermal reduction may have the possibility of forming cross-links between adjacent RGO at defects, which helps to construct highly dense RGO films, leading to high electrical conductivity. The thin (~4 μm thick), freestanding and highly conductive RGO film with a low sheet resistance of 0.8 Ω/sq can be employed to use as ultralight current collectors for lithium-ion batteries.

Starting with graphite, a GO dispersion was prepared by an improved Hummer's method,[33] which was then filtrated to achieve a freestanding GO film with a controlled thickness. Before Joule heating, the GO film was thermally reduced at 773 K in argon (Ar) to preanneal the GO. The preannealed RGO had relatively low conductivity, which was used to trigger the Joule heating by applying electrical current. The temperature of the RGO film increased with applied dc bias, which was monitored through an optical fiber coupled in the homemade setup. During the Joule heating process, a high temperature (2750 K) was detected, which thermally reduced the graphene oxide within minutes, leaving a highly conductive RGO film.

DOI: 10.1021/acs.nanolett.6b00743
Nano Lett. 2016, 16, 3616−3623

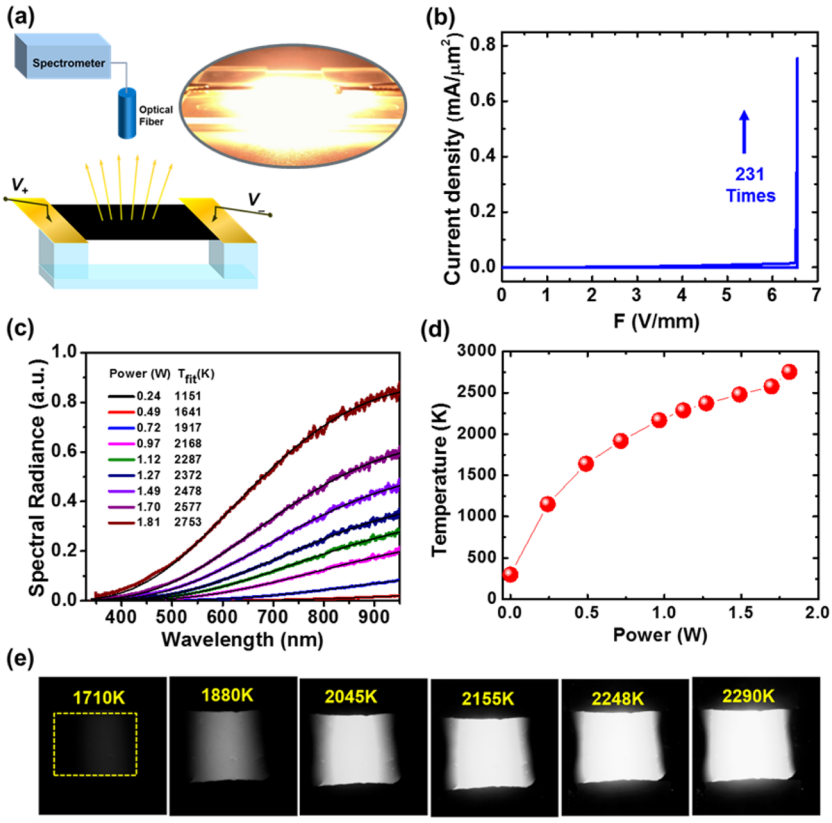

Figure 2. (a) Experiment setup for carrying out the Joule heating experiment in a vacuum chamber with a spectrometer and coupled optical fiber. The bright image is a RGO film under 4 V bias voltage. (b) Current density versus applied electrical field during the Joule heating process for a RGO sample which was preannealed at 773 K for 1 h. Note that the current density increases by 231 times in the sample. (c) Spectral radiance measurement of the same sample with different electrical power inputs. Temperature is determined by fitting the spectra to Planck's law assuming constant emissivity (solid black curves). (d) Fitted temperature of the RGO film versus input electrical power. (e) Sequence of camera images showing the RGO film heating process with increasing applied electrical power. The white part is the illuminated area radiating due to the high temperature induced by electrical current.

Our experimental analysis confirms that most of the defects were removed after the high-temperature process (Figure 1a). Raman spectroscopy was used to study the structural changes of GO before and after Joule heating. Compared to the preannealed GO film (Figure 1b), the D peak of the Joule-heated RGO film associated with the defective carbon (1350 cm^{-1}) is dramatically decreased and the G peak associated with crystalline carbon (1600 cm^{-1}) remains as a high intensity sharp peak (Figure 1c), producing a significant decrease in the ratio of the D mode over G mode (I_D/I_G) from 1.02 to 0.02.

The decreased I_D/I_G ratio indicates that the Joule-heated RGO film can become highly crystallized, with a structural transformation from amorphous carbon to crystallized carbon. In addition, a sharp 2D peak (2690 cm^{-1}) can be observed after Joule heating, with an I_{2D}/I_G ratio of 0.93, confirming the highly crystalline structure of the RGO film after the Joule heating process.[34,35] The characteristic peaks of the Raman spectroscopy show that a highly reduced GO film can be obtained by employing electrical current to generate Joule heating, leading to superior electrical conductivity of the RGO film. The ex situ Raman spectra from the Joule heating process is investigated in detail in the Supporting Information.

Cross-section scanning electron microscopy (SEM) images of the RGO film (Figure 1d,e) reveal a dense structure after the Joule heating compared to pristine. The preannealed GO film shows that stacked RGO layers can be clearly observed with a thickness of 1.25 μm before Joule heating. After electrical current annealing at 2750 K for 1 min in vacuum, the thickness of RGO film decreased to 1.03 μm, exhibiting a relatively dense fracture surface (Figure 1e). The morphology difference may come from the highly stacked RGO flakes that were "melted" or "welded" together during Joule heating at the areas of highest temperature. This densification of RGO flakes is possibly due to the extremely high temperature generated by the current-induced high thermal energy on the junction points of surrounding RGO flakes as well as defects on the surface. The high crystallinity of the RGO nanosheets (increased conduction within each nanosheets) and their dense structure (increased conduction between flakes) simultaneously achieve the record high electrical conductivity of 3112 S/cm.

We investigate the Joule heating process by using the setup shown in Figure 2a. The setup is used to measure the temperature of samples by recording the emitted light during the Joule heating process. In this setup, the preannealed GO film was suspended above a substrate and the two ends of film were bonded by silver paste to connect two copper electrodes. The Joule heating was conducted by applying direct current (dc) through the preannealed GO sample (773 K for 1 h) in a vacuum chamber. The RGO film shines brightly when electrical current is applied. The bright emission, close to white in color, indicates that extreme high temperature is achieved (Figure S1). During the Joule heating, some key parameters including voltage, current, and radiation spectrum were collected to study the thermal behavior of the RGO sample. The spectrometer

DOI: 10.1021/acs.nanolett.6b00743
Nano Lett. 2016, 16, 3616−3623

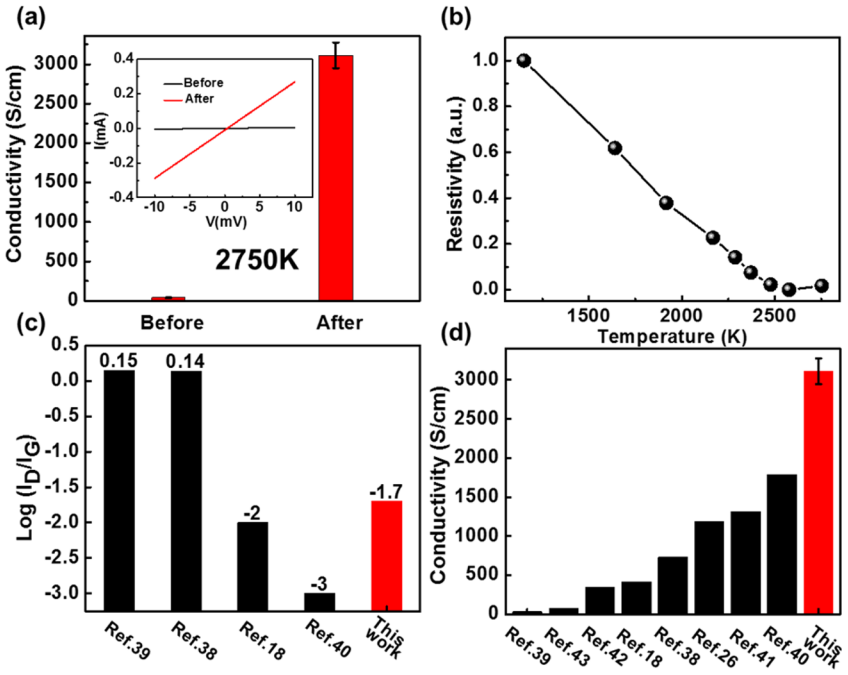

Figure 3. (a) Conductivity of RGO film before and after the 2750 K reduction by the Joule heating. Inset shows the linear scan of the $I-V$ curve. (b) Resistance versus temperature of RGO film during the Joule heating process. (c) Log value of intensity ratio of D peak (1350 cm^{-1}) to G peak (1600 cm^{-1}) (I_D/I_G) of RGO films by different reduction method. (d) The dc conductivity of graphene and RGO nanostructures reported by literatures.

coupled optical fiber having a diameter of 400 μm was placed on top of the RGO sample. The optical fiber and the RGO film have a distance of 15 cm to collect the light emission. Current density was recorded as the applied voltage on the preannealed RGO was increased (Figure 2b). The current density increased slowly with the applied voltage on the RGO film. When the voltage was increased to 6.55 V/mm, the current density instantaneously increased from 0.0033 to 0.76 mA/μm^2, which is around 200 times higher. The significant increase in the conductivity is possibly due to the removal of defects and impurities in RGO film during the high temperature induced by Joule heating.

To characterize the temperature of the RGO films under given voltages, their corresponding emission spectra were recorded by the spectrometer coupled optical fibers, as shown in Figure 2c. The emission spectrum in the wavelength range of 340 to 950 nm was recorded by a spectral measurement system, calibrated by a NIST-traceable light source to ensure accuracy of the measurement. The effect of the glass window of the vacuum chamber has been excluded. The recorded emission spectrum of the RGO film under high temperature was then fitted to the blackbody radiation equation as shown below to extract the in situ temperature of the RGO film

$$I_\lambda(\lambda, T) = \gamma \varepsilon_{gray} \frac{2hc^2}{\lambda^5 \left[\exp\left(\frac{hc}{\lambda k_B T}\right) - 1\right]} \quad (1)$$

where k_B is the Boltzmann constant, h is the Planck constant, c is the speed of light, and γ is the scaling constant taking consideration of the unknown coupling factor between the RGO film illumination and the input of the optical fiber. ε_{gray} is a constant emissivity. By a mathematical fitting of each curve from Figure 2c to eq 1, the sample temperature can be extracted.[36,37] Figure 2d shows the results of the fitted temperatures (T) as a function of applied electrical power (P). Note that 2750 K was the highest temperature obtained by the power supply device in our setup. We envision that a higher temperature can be achieved if a higher power can be applied to the RGO samples. Figure 2e displays a series of images of RGO film taken under different levels of electrical power during the Joule heating process. Each image has an average exposure time of 100 ms. The white part is the illuminated area. The input Joule heating energy is equal to the thermal conduction of the metal contacts on both ends and the blackbody radiation. As the input power increases, the areas exhibiting blackbody radiation become more visible in the images, as appears in the bright areas of Figure 2e, indicating a higher temperature was generated.

The electrical conductivity of RGO before and after high temperature reduction at 2750 K was measured. The slope of the linear scan in Figure 3a shows that the conductivity increases from ~40 to 3023 S/cm with a 76-fold increase. The sample has a size of 2043 μm long, 212 μm wide, and 1.03 μm thick. To obtain accurate values 10 samples were measured and their experimental results were averaged with conductivity value of 3112 ± 164 S/cm. The resistivity versus the reduction temperature during the Joule heating process was recorded (Figure 3b). The large increase in dc conductivity is due to the improved crystallinity upon the high-temperature treatment, which can be confirmed by the Raman results as well (shown in Figure 1). Note that our I_D/I_G ratio in the Raman spectroscopy after the Joule heating became much lower than reported data in the literature.[18,38−40] Our RGO film reduced at a high temperature with a low I_D/I_G ratio shows a much higher dc conductivity (Figure 3d, Table S1) than RGO films prepared by chemical reduction or thermal reduction.[18,26,38−43] According to literature, Li et al. reported a chemically reduced RGO film with an I_D/I_G ratio of 1.38 and dc conductivity of 33 S/cm,[39] and Mullen et al. reported thermally reduced RGO film with an I_D/I_G ratio of 1.4 S/cm and dc conductivity of 727 S/cm.[38] Recently, Lian et al. reported that a high processing

DOI: 10.1021/acs.nanolett.6b00743
Nano Lett. 2016, 16, 3616−3623

temperature up to 3123K was used to anneal their heterogeneous microsized fiber with RGOs of two different sizes.[40] Their higher temperature leads to an even lower I_D/I_G ratio of ~0.001 for pure RGOs (Figure 3c). It is interesting that our dc conductivity of 3112 S/cm is much higher than the value 1790 S/cm they achieved for pure RGOs, although their I_D/I_G ratio is lower than ours.

The increased dc conductivity is explained to the possibility that the Joule heating in our process can selectively reduce the high-resistance, defect regions which then self-heal the defect structure. Note the temperature of 2750 K is obtained through fitting the macroscopic blackbody radiation. Local heating with a much higher temperature may possibly generate, although this part of heat cannot be detectable by the radiation spectrum measurement. The local heating at a high temperature in the RGO film, especially in the contact area between RGO nanosheets, could potentially "weld" the RGO nanosheets together through defective carbon atoms to form a 3D cross-linked carbon nanostructure.

The morphology and chemical compositions of RGO films were investigated to understand the record high dc conductivity. Figure 4a,b shows the surface morphology of RGO film before and after the Joule heating, respectively. Magnified morphologies are given in each inset of the SEM images. The RGO film surface becomes much smoother after the 2750 K reduction. Note that the cross-section SEM shown in Figure 1 reveals that high-temperature reduction can increase the stacking density of the RGO layers. Both the top and cross-section views show the high-temperature process can effectively remove irregularities in the structure. TEM images with an obvious crystalline lattice (Figure S3) reveal the highly crystalline graphene structure of the 2750 K Joule-heated RGO film. The selected-area electron diffraction (SAED) yielding patterns match with those expected for multilayer graphene flakes. Furthermore, the filtered image (Figure S3c) clearly suggests that the 2750 K Joule-heated RGO film shows a high crystallinity with few defects. For the control sample, the 1700 K Joule-heated RGO film shows a poor crystallinity (Figure S4).

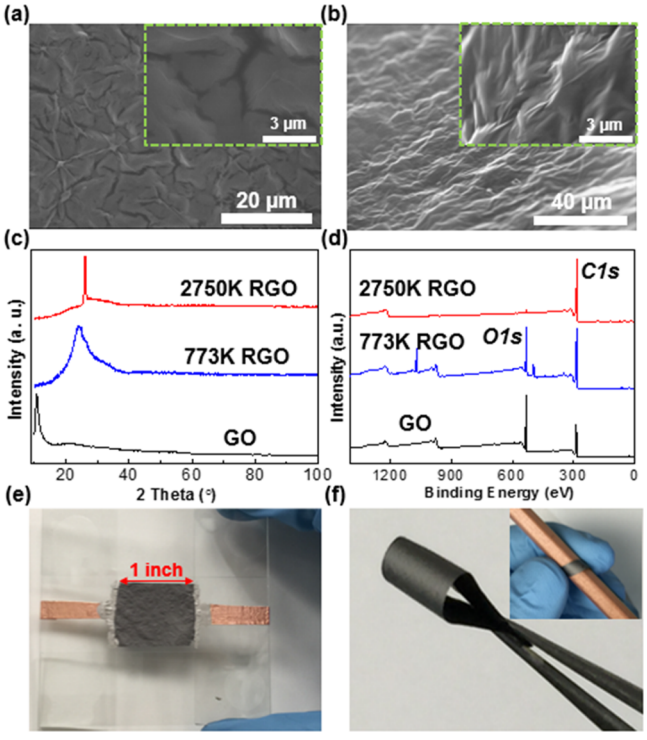

Figure 4. (a) Surface morphology of preannealed GO film. Inset: detail of surface morphology at higher magnification. (b) Surface morphology of the high-temperature reduced RGO film after Joule heating. Inset: detail of surface morphology at higher magnification. (c) XRD patterns of GO, RGO after annealing for 1 h at 773 K (preannealing) and RGO after annealing at 2750 K by Joule heating. (d) XPS scans of the same samples as in (c). (e) A 1 in. × 1 in. RGO sample reduced by the high-temperature process. (f) The high-temperature, Joule-heated RGO is mechanically flexible. Inset: RGO film was bent around a regular pencil.

X-ray diffraction (XRD) and X-ray photoelectron spectroscopy (XPS) were employed to investigate the microstructure of GO, thermally reduced RGO at 773 K (preannealed), and high-temperature annealed RGO at 2750 K by the Joule heating method. The characteristic peak corresponding to (002) in graphite shows up around ~26.58° after the thermal reduction of GO at 773 K (Figure 4c). After high-temperature reduction by Joule heating, the characteristic peak becomes much more narrow and sharp. On the basis of the peak position, the RGO layer–layer distance was obtained, which decreases from 0.369 nm for 773 K reduction to 0.341 nm for 2750 K reduction. The *d*-spacing decrease is due to the effective removal of the functional groups in RGO film. Note that the *d*-spacing is close to the value of graphite (~0.334 nm).[44] The narrow peak at 26.58° indicates that the uniform stacking space in 2750 K RGO is due to the even distribution of current in the RGO film during the Joule heating reduction. XPS scans of the three types of samples were carried out as shown in Figure 4d. The carbon to oxygen atomic ratio is 2.8 in GO, 3.55 in 773 K RGO, and 81.64 in 2750 K RGO, which confirms the effective removal of the functional groups. Note that the 2750 K temperature was only held for 1 min in our experiment to achieve high quality RGO film, which is attractive for fast nanomanufacturing. We demonstrated one RGO film with a size of 1 in. × 1 in. through solution filtration and 1 min high-temperature reduction (Figure 4e). The RGO film is highly flexible, which can be bent down to a small radius with no cracking (Figure 4f).

We attribute the drastic increase in the electrical conductivity of the RGO film after high temperature annealing to the following underlying mechanism: under increasing temperature, the defects in RGO nanolayers (e.g., vacancies, grain boundaries, voids, line defects, and so forth) facilitate the formation of interlayer bridging bonds between neighboring RGO layers, which in turn effectively leads to substantial enhancement of the electrical conductivity of the RGO film. To validate the above-proposed mechanism, we carried out molecular dynamics simulations to model the cross-linking process of neighboring RGO layers (see extended simulation details and results in Supporting Information). For simplicity, we considered a bilayer graphene model with three parallel line defects of width about 0.48 nm in each layer but at different locations (Figure 5a). The bilayer graphene structure is first heated up from 300 to 2500 K in 400 ps, then maintained at 2500 K for 400 ps. During the heating process from 300 to 1420 K, the thermal fluctuation drives the interlayer sliding between the top and bottom graphene layers, suggesting that the interlayer interaction is largely nonbonded type (i.e., van der Waals forces). However, at higher temperatures interlayer bridging bonds start to form when the line defects in two graphene layers come close to each other facilitated by

DOI: 10.1021/acs.nanolett.6b00743
Nano Lett. 2016, 16, 3616–3623

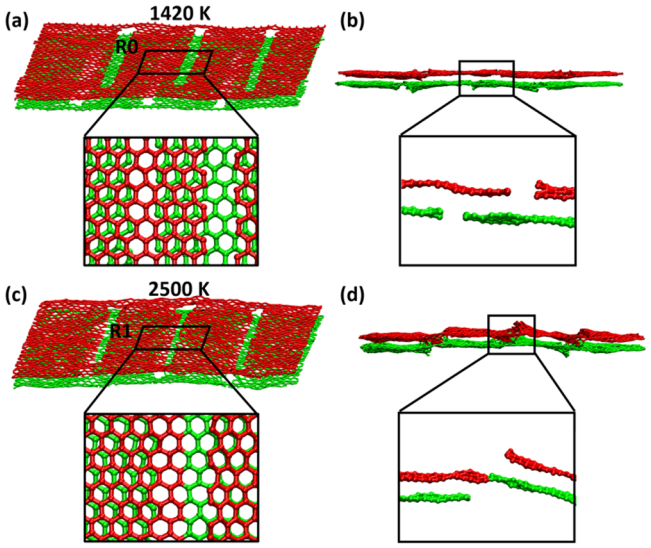

Figure 5. Molecular dynamics simulations demonstrate the defect-facilitated formation of interlayer bridging bonds between two defective neighboring graphene layers at high temperatures. Three parallel line defects exist in each layer (top: red; bottom: green). (a) At 1420 K, the two graphene layers remain separated with no interlayer bridging bond formation. Inset shows the zoomed-in top view of region R0 near the line defects. (b) Side view of (a). Inset shows the zoomed-in cross-section view of region R0. (c) At 2500 K, covalent interlayer bridging bonds form. (d) The side view of (c). Both insets in (c) and (d) clearly show that the left edge of the line defect in the top graphene layer is covalently bonded to the right edge of the neighboring line defect in the bottom graphene layer.

interlayer sliding. Figure 5 plots the snapshot of the bilayer graphene structure at two representative temperatures: at 1420 K (Figure 5a,b), the top and bottom graphene layers remain separated by the equilibrium interlayer distance (0.34 nm) without interlayer bridging bond formation; and at 2500 K, however, covalent interlayer bridging bonds form at the line defects. As clearly shown in Figure 5d, the left edges of all three line defects in the top graphene layer are bonded to the right edges of the neighboring line defects in the bottom graphene layer. The defect-facilitated interlayer bridging bond formation can be attributed to the enhanced reactivity of carbon atoms at the defect edge due to available dangling bonds. High temperatures further increase the reactivity of such carbon atoms with dangling bonds and could also result in migration of defects within the layer, which further facilitates the interlayer bridging bond formation. As a result, the resulting RGO film after high-temperature annealing is expected to be highly cross-linked via rich interlayer bridging bonds, leading to the drastic increase of electrical conductivity. The above modeling results agree with recent work by Barreiro et al. that two overlapped graphene nanosheets can be healed together at high temperature[45] and by Zhang and Li that interlayer bridging bonds can form in a carbon nanoscroll made by rolling up a graphene layer with patterned point defects followed by heating up to a high temperature.[46]

The highly conductive, flexible RGO film with a conductivity of over 3000 S/cm from solution processed GO ink can enable a range of applications from transparent electrodes[16] to current collectors in various batteries. In this work, we demonstrate the highly conductive RGO film as an ultralight current collector

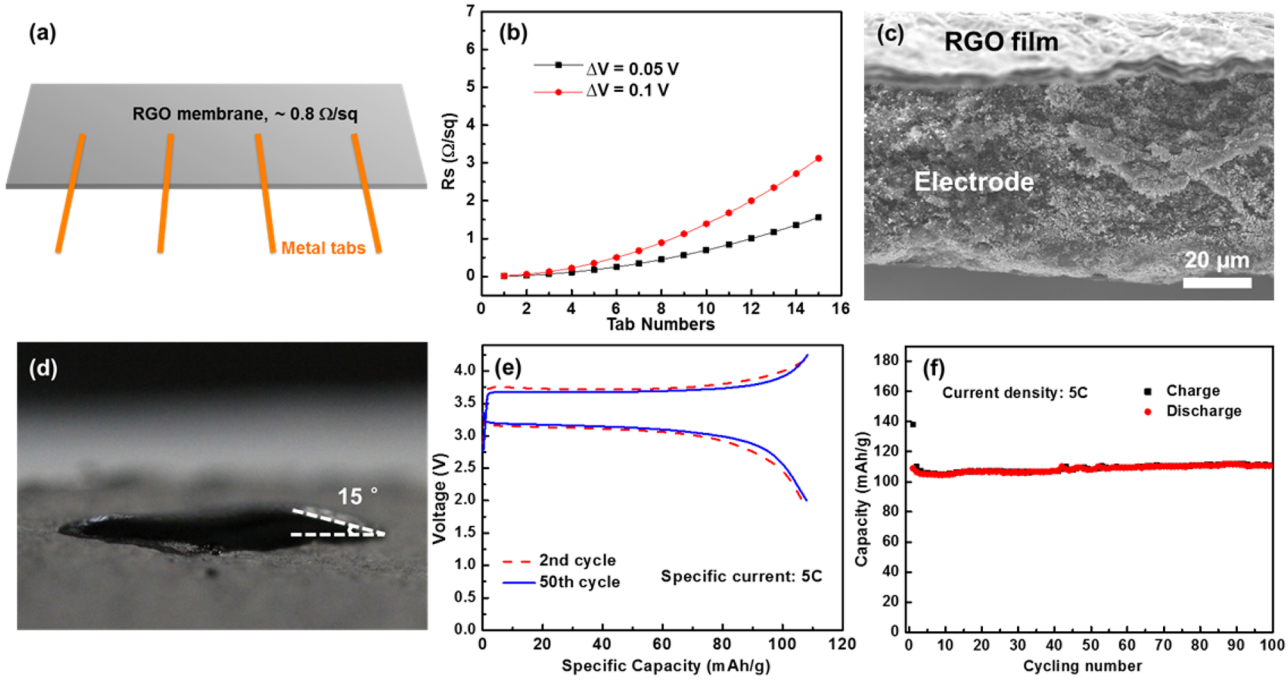

Figure 6. (a) Schematic to show the metal tabs on top of the RGO current collector in an unrolled battery electrode. Note that typical length of a 18 650 cell is 600 mm and width is 50 mm. The metal tabs are designed to conduct the current out. (b) Relationship between sheet resistance and number of tabs in a 18 650 cell with a current density of 2 mA/cm^2. The values of the overpotential (0.05 and 0.1 V) are due to the resistance of the current collector. Number of tabs decreases as the sheet resistance of the current collector decreases. (c) SEM image of a $LiFePO_4$ composite cathode coated on a RGO current collector, showing excellent contact. (d) Digital image of a $LiFePO_4$ slurry droplet on RGO film with a small contact angle of 15°, illustrating excellent wetting and adhesion properties at the electrode/RGO interface. (e) Galvanostatic discharge/charge profiles of the $LiFePO_4$ electrode with RGO film current collector for the 2nd and 50th cycles. These tests were conducted in the potential range of 2−4.5 V versus Li/Li$^+$ at 5C. (f) Cycling performance of the $LiFePO_4$ electrode with RGO film current collector at 5C.

DOI: 10.1021/acs.nanolett.6b00743
Nano Lett. 2016, 16, 3616−3623

for lithium-ion batteries, where we did initial calculation on the dimensions of the current collectors based on a standard 18 650 cell configuration (see details in Supporting Information). To minimize the IR drop, metal tabs were typically used on the top of the current collectors to conduct global current, which conduct primarily local current (Figure 6a). Here we calculated the dependence of IR drop with the number of tabs and the sheet resistance of the current collector (Figure 6b). For example, when the current density is 2 mA/cm^2, only 11 metal tabs were required with a spacing of 54.5 mm spacing to keep a negligible IR drop of 0.05 V, considering the sheet resistance of RGO film is as low as 0.8 Ω/sq.

The RGO film current collector was demonstrated by constructing a cathode electrode as shown in Figure 6c. A slurry composed of lithium iron phosphate ($LiFePO_4$, LFP), carbon black, and binder (polyvinylidene fluoride, PVdF) with a mass ratio of 7:2:1 was prepared, cast onto the RGO film, and finally dried in a vacuum oven overnight at 373 K to obtain the electrode. The electrode had thickness of ∼70 μm and LFP mass loading of 7 mg/cm^2. Figure S7 shows a magnified SEM of the interface between the electrode and the RGO current collector. The dense interface indicates that the dried cathode and RGO formed a good contact in between, which provides good electron transfer pathway between electrode and current collector. The wettability of the RGO film with the fresh slurry ink is shown in Figure 6d. The small contact angle, which is ∼15° between the slurry ink and the RGO film, confirms the superior wettability of RGO film. In addition, the rough RGO film surface provides extra surface area for the slurry ink to wet, and such an increase in the surface area can be able to enhance the electrochemical properties of the electrode when high current is applied. The electrochemical performance of the electrode with a RGO film current collector is shown in Figure 6e, which exhibited a smaller polarization in terms of voltage difference between the plateaus of the charge and discharge curves, compared to the electrode that used an Al current collector (Figure S8). A high specific current 5C (1C = 170 mA/g) was applied and the cell with a loading density of 7 mg/cm^2 delivered a capacity of ∼110 mAh/g. The cycling performance in Figure 6f exhibits no capacity decay in the measured 100 cycles. Cyclic voltammetry (CV) measurement was used to study the electrochemical stability of the RGO film at high voltage. The result showed good electrochemical stability of RGO film at 4 V (Figure S9). Its good electrochemical performance indicates that the highly conductive, lightweight RGO film can be potentially used as a current collector to replace conventional metal-based current collectors. Meanwhile, the RGO film provides increased surface area to physically contact with electrode so as to improve the interfacial bonding and electrochemical performance. To demonstrate the mechanical stability of RGO film in liquid electrolyte, RGO films were soaked in ethylene carbonate/diethyl carbonate (EC/DEC = 1:1 by volume) solution for 3 days, followed by vacuum drying at 80 °C to measure its mechanical property. Results show that the RGO film still exhibits high flexibility and high tensile strength with a value of 20.1 MPa (Figures S10−S13). In addition, RGO films were wetted by organic solvent *N*-methyl-2-pyrrolidone (NMP) to mimic the real operation of electrode slurry coating process to check the stability of RGO films in this process. As shown in Figure S14, the RGO film maintained good flexibility and stable structure without swelling after NMP wetting, indicating the compatibility of RGO current collector with commercial slurry coating process.

CONCLUSION

In this work, we report a highly conductive RGO film with record-high dc conductivity up to 3112 S/cm. The highly conductive RGO film is fabricated by a solution based filtration process followed by thermal reduction (773 K) and then a high-temperature reduction (2750 K by Joule heating). The unique high-temperature reduction by Joule heating can effectively remove defects from graphene oxide, improve the crystalline structure of individual RGO nanosheets, and densify their stacking in between, leading to a 231-fold increase in dc conductivity. The drastically increased electrical conductivity of RGO films after high-temperature annealing is attributed to the defect-facilitated cross-linking of neighboring RGO layers, as confirmed by our molecular dynamics simulations. The highly conductive RGO film can have a wide range of applications from microelectronics to large-scale printed electronics. We successfully employed the highly conductive RGO films as current collectors in Li-ion batteries. We envision that the simple but effective Joule heating method can provide a new tool to study and investigate materials under extreme thermal conditions.

ASSOCIATED CONTENT

Supporting Information

The Supporting Information is available free of charge on the ACS Publications website at DOI: 10.1021/acs.nanolett.6b00743.

Experimental details for material preparation and characterization, Joule heating process and characterization, molecular dynamics simulations, calculation on the dimensions of current collectors, and electrochemical and mechanical evaluations. (PDF)

AUTHOR INFORMATION

Corresponding Author

*E-mail: binghu@umd.edu.

Author Contributions

Y.C. and K.F. contributed equally.

Notes

The authors declare no competing financial interest.

ACKNOWLEDGMENTS

Dr. Hu acknowledges the financial support from the dean's office for the equipment setup. We acknowledge the support of the Maryland NanoCenter and its NispLab. Y.C. acknowledges China Scholarship Council (CSC) for financial support.

REFERENCES

(1) Johnson, B. A.; White, R. E. *J. Power Sources* **1998**, *70*, 48−54.

(2) Myung, S.-T.; Hitoshi, Y.; Sun, Y.-K. *J. Mater. Chem.* **2011**, *21*, 9891−9911.

(3) Braithwaite, J. W.; Gonzales, A.; Nagasubramanian, G.; Lucero, S. J.; Peebles, D. E.; Ohlhausen, J. A.; Cieslak, W. R. *J. Electrochem. Soc.* **1999**, *146*, 448−456.

(4) Zhou, R.; Meng, C.; Zhu, F.; Li, Q.; Liu, C.; Fan, S.; Jiang, K. *Nanotechnology* **2010**, *21*, 345701.

(5) Park, S.; Shim, H.-W.; Lee, C. W.; Song, H. J.; Park, I. J.; Kim, J.-C.; Hong, K. S.; Kim, D.-W. *Nano Res.* **2015**, *8*, 990−1004.

DOI: 10.1021/acs.nanolett.6b00743
Nano Lett. 2016, 16, 3616−3623

(6) Yazici, M. S.; Krassowski, D.; Prakash, J. *J. Power Sources* **2005**, *141*, 171−176.
(7) Hu, L.; Wu, H.; La Mantia, F.; Yang, Y.; Cui, Y. *ACS Nano* **2010**, *4*, 5843−5848.
(8) Choi, J. W.; Hu, L.; Cui, L.; McDonough, J. R.; Cui, Y. *J. Power Sources* **2010**, *195*, 8311−8316.
(9) Lytle, J. C.; Wallace, J. M.; Sassin, M. B.; Barrow, A. J.; Long, J. W.; Dysart, J. L.; Renninger, C. H.; Saunders, M. P.; Brandell, N. L.; Rolison, D. R. *Energy Environ. Sci.* **2011**, *4*, 1913−1925.
(10) Hu, L.; Hecht, D. S.; Grüner, G. *Nano Lett.* **2004**, *4*, 2513−2517.
(11) Qu, L.; Vaia, R. A.; Dai, L. *ACS Nano* **2011**, *5*, 994−1002.
(12) Hecht, D. S.; Hu, L.; Irvin, G. *Adv. Mater.* **2011**, *23*, 1482−1513.
(13) Wang, K.; Luo, S.; Wu, Y.; He, X.; Zhao, F.; Wang, J.; Jiang, K.; Fan, S. *Adv. Funct. Mater.* **2013**, *23*, 846−853.
(14) Han, X.; Chen, Y.; Zhu, H.; Preston, C.; Wan, J.; Fang, Z.; Hu, L. *Nanotechnology* **2013**, *24*, 205304.
(15) Lin, X.; Shen, X.; Zheng, Q.; Yousefi, N.; Ye, L.; Mai, Y.-W.; Kim, J.-K. *ACS Nano* **2012**, *6*, 10708−10719.
(16) Zhao, J.; Pei, S.; Ren, W.; Gao, L.; Cheng, H.-M. *ACS Nano* **2010**, *4*, 5245−5252.
(17) Xu, Z.; Zhang, Y.; Li, P.; Gao, C. *ACS Nano* **2012**, *6*, 7103−7113.
(18) Cruz-Silva, R.; Morelos-Gomez, A.; Kim, H.; Jang, H.; Tristan, F.; Vega-Diaz, S.; Rajukumar, L. P.; Elías, A. L.; Perea-Lopez, N.; Suhr, J.; Endo, M.; Terrones, M. *ACS Nano* **2014**, *8*, 5959−5967.
(19) Jang, H. D.; Kim, S. K.; Chang, H.; Choi, J.-H.; Cho, B.-G.; Jo, E. H.; Choi, J.-W.; Huang, J. *Carbon* **2015**, *93*, 869−877.
(20) Han, T. H.; Huang, Y.-K.; Tan, A. T. L.; Dravid, V. P.; Huang, J. *J. Am. Chem. Soc.* **2011**, *133*, 15264−15267.
(21) Wu, Z. S. *ACS Nano* **2009**, *3*, 411−417.
(22) Pei, S. *Carbon* **2010**, *48*, 4466−4474.
(23) Moon, I. K.; Lee, J.; Ruoff, R. S.; Lee, H. *Nat. Commun.* **2010**, *1*, 73.
(24) Williams, G.; Seger, B.; Kamat, P. V. *ACS Nano* **2008**, *2*, 1487−1491.
(25) Cote, L. J.; Cruz-Silva, R.; Huang, J. *J. Am. Chem. Soc.* **2009**, *131*, 11027−11032.
(26) Pei, S.; Cheng, H.-M. *Carbon* **2012**, *50*, 3210−3228.
(27) Bagri, A.; Mattevi, C.; Acik, M.; Chabal, Y. J.; Chhowalla, M.; Shenoy, V. B. *Nat. Chem.* **2010**, *2*, 581−587.
(28) Mann, D.; Kato, Y. K.; Kinkhabwala, A.; Pop, E.; Cao, J.; Wang, X.; Zhang, L.; Wang, Q.; Guo, J.; Dai, H. *Nat. Nanotechnol.* **2007**, *2*, 33−38.
(29) Liu, P.; Sun, Q.; Zhu, F.; Liu, K.; Jiang, K.; Liu, L.; Li, Q.; Fan, S. *Nano Lett.* **2008**, *8*, 647−651.
(30) Cao, Q.; Rogers, J. A. *Adv. Mater.* **2009**, *21*, 29−53.
(31) Ishikawa, F. N.; Curreli, M.; Olson, C. A.; Liao, H.-I.; Sun, R.; Roberts, R. W.; Cote, R. J.; Thompson, M. E.; Zhou, C. *ACS Nano* **2010**, *4*, 6914−6922.
(32) Wang, C.; Zhang, J.; Ryu, K.; Badmaev, A.; De Arco, L. G.; Zhou, C. *Nano Lett.* **2009**, *9*, 4285−4291.
(33) Marcano, D. C.; Kosynkin, D. V.; Berlin, J. M.; Sinitskii, A.; Sun, Z.; Slesarev, A.; Alemany, L. B.; Lu, W.; Tour, J. M. *ACS Nano* **2010**, *4*, 4806−4814.
(34) Ferrari, A. C.; Basko, D. M. *Nat. Nanotechnol.* **2013**, *8*, 235−246.
(35) Dresselhaus, M. S.; Jorio, A.; Hofmann, M.; Dresselhaus, G.; Saito, R. *Nano Lett.* **2010**, *10*, 751−758.
(36) Kim, Y. D.; Kim, H.; Cho, Y.; Ryoo, J. H.; Park, C.-H.; Kim, P.; Kim, Y. S.; Lee, S.; Li, Y.; Park, S.-N.; Shim Yoo, Y.; Yoon, D.; Dorgan, V. E.; Pop, E.; Heinz, T. F.; Hone, J.; Chun, S.-H.; Cheong, H.; Lee, S. W.; Bae, M.-H.; Park, Y. D. *Nat. Nanotechnol.* **2015**, *10*, 676−681.
(37) Freitag, M.; Chiu, H.-Y.; Steiner, M.; Perebeinos, V.; Avouris, P. *Nat. Nanotechnol.* **2010**, *5*, 497−501.
(38) Wang, X.; Zhi, L.; Müllen, K. *Nano Lett.* **2008**, *8*, 323−327.
(39) Yang, X.; Cheng, C.; Wang, Y.; Qiu, L.; Li, D. *Science* **2013**, *341*, 534−537.
(40) Xin, G.; Yao, T.; Sun, H.; Scott, S. M.; Shao, D.; Wang, G.; Lian, J. *Science* **2015**, *349*, 1083−1087.
(41) Su, Q.; Pang, S.; Alijani, V.; Li, C.; Feng, X.; Müllen, K. *Adv. Mater.* **2009**, *21*, 3191−3195.
(42) Chen, H.; Müller, M. B.; Gilmore, K. J.; Wallace, G. G.; Li, D. *Adv. Mater.* **2008**, *20*, 3557−3561.
(43) Li, D.; Müller, M. B.; Gilje, S.; Kaner, R. B.; Wallace, G. G. *Nat. Nanotechnol.* **2008**, *3*, 101−105.
(44) Pierson, H. O. *Handbook of Carbon, Graphite, Diamonds and Fullerenes: Processing, Properties and Applications*; William Andrew: New York, 2012.
(45) Barreiro, A.; Börrnert, F.; Rümmeli, M. H.; Büchner, B.; Vandersypen, L. M. K. *Nano Lett.* **2012**, *12*, 1873−1878.
(46) Zhang, Z.; Li, T. *Nanoscale Res. Lett.* **2011**, *6*, 470.

DOI: 10.1021/acs.nanolett.6b00743
Nano Lett. 2016, 16, 3616−3623